This journal is © The Royal Society of Chemistry 2013

Materials and Methods

S-I. The synthesis and XRD characterization of T-ZnO and R-ZnO

Tetrapod-shaped ZnO nanopowders (named as T-ZnO) were prepared by the method of vapor-phase oxidation from metallic zinc as raw materials. The metallic zinc was melted by induction heating in a vacuum chamber with a flowing gas mixture of Ar+O_2, and then ZnO powders were formed by metallic zinc vapor oxidating, finally the ZnO powders condensed on water-cooled wall of the chamber. The tetrapod-shaped ZnO nanoparticles can be obtained by controlling the temperature of induction heating and the pressure of Ar and O_2, which has been reported in our previous work.[1] ZnO nanorods (denoted as R-ZnO) were synthesized by a facile wet-chemical approach according to Liu's work.[2] The alkali solution of zinc was prepared by dissolving 14.87 g of zinc nitrate [$Zn(NO_3)_2 \cdot 6H_2O$] and 40.00 g of NaOH in deionized water to form a 100.0 mL solution ([Zn^{2+}] = 0.50 M, [OH^-] = 10.00 M; molar ratio of Zn^{2+}:OH^- = 1:20). Three milliliters of the above solution was then mixed with 0.0-5.0 mL of deionized water and 25.0-30.0 mL of pure alcohol (C_2H_5OH), followed by adding 5.0-6.0 mL of ethylenediamine ($C_2H_4(NH_2)_2$, EDA; molar ratio of Zn^{2+}:EDA = ca. 1:50 to 1:60). Before being transferred to a Teflon-lined autoclave, the solution mixture was pretreated under an ultrasonic water bath for 20-40 min. The hydrothermal syntheses were conducted at 180 °C for 20 h in an electric oven. After the reactions, white crystalline products (ZnO nanorods) were harvested by centrifugation and thorough washings with deionized water.

Figure S1 shows the XRD patterns of T-ZnO and R-ZnO, it can be seen that all diffraction peaks of both samples were in good agreement with the standard data for ZnO (JCPDS 36-1451) and the sharp diffraction peaks implied complete crystal structure. No impurity peaks were detected. These results indicated that T-ZnO and R-ZnO crystallized in a pure hexagonal wurtzite structure. In addition, the relative intensity of diffraction peaks of R-ZnO was much larger than that of T-ZnO because R-ZnO had better crystalline and exhibited more complete facets.

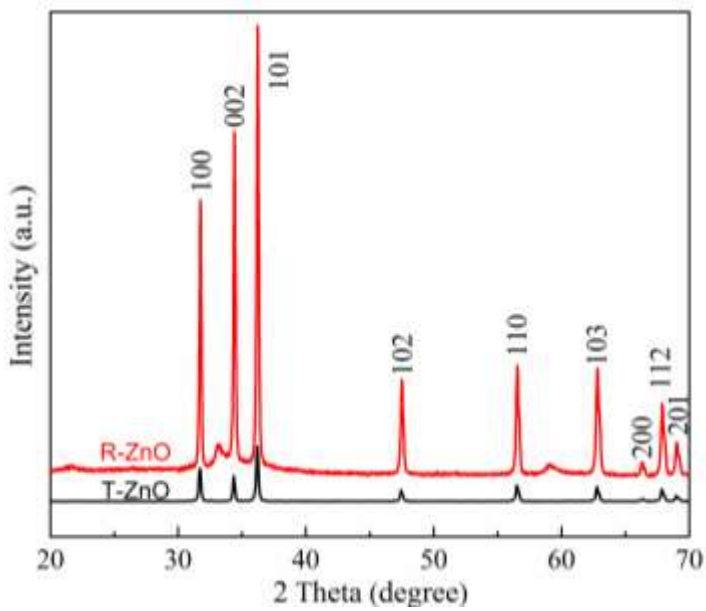

Figure S1. XRD patterns of T-ZnO and R-ZnO.

S-II. DFT Calculations and Surface Model Details

DFT calculations were carried out using plane waves as implemented in Vienna Ab-initio Simulation Package.[3-5] The cutoff energy of the electronic wave functions were expanded to 400 eV and projected augmented wave function (PAW) pseudopotentials[6] were used to describe electron-ion interactions. The Perdew-Burke-Ernzerhof (PBE) functional[7] was used as exchange- correlation functional. The geometry optimization is considered complete when the Hellmann-Feynman force on each atom is less than 0.05 eV/Å. A climbing nudged elastic band (NEB) calculations[8,9] is used to calculate the minimum energy path (MEP) and find the saddle points between two local minima for the system.

The PA decomposition on nano-ZnO $(10\bar{1}0)$ surface was investigated by DFT calculations. Figure S2(a) shows bulk structure of ZnO in this study. The calculated period along the [0001] direction of ZnO in bulk phase is 5.21 Å, in good agreement to experimentally measured *c*-axis period of 5.2 Å in bulk phase. A periodic $(10\bar{1}0)$ slab model was cleaved from bulk ZnO with a thickness of six atomic layers, such that the bottom two atomic layers were fixed at their bulk positions. An orthorhombic supercell with area of 5.2×6.5 $Å^2$ was used to investigate the PA adsorption on the ideal $(10\bar{1}0)$ surface

(Figure S2(b)) and a vacuum layer of 10 Å was added to avoid intermolecular interactions. To model a stepped structure along [0001] direction, a larger slab was generated with size of 15.6×9.7 $Å^2$ and a groove with width of 8.5 Å and depth of 3.0 Å along *b*-axis on the slabs was created (Figure S2(c)). In order to passivate the surface slab, we used pseudo-hydrogen atoms with a non-integer core charge of 1.5 and 0.5 for Zn and O, respectively, which has been shown to be effective in eliminating the surface states within the band gap from previous literatures.[10,11] The K-points were sampled in a Monkhosrt-Pack (MP) mesh of 4×4×1 for Brillouin zone integration and the total energy convergence was well tested.

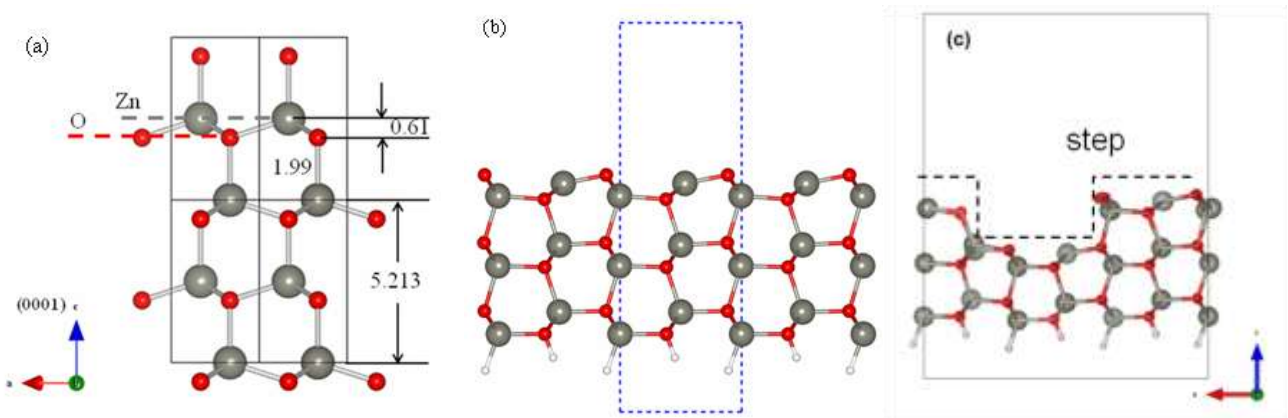

Figure S2. (a), (b) and (c) show bulk structure, surface and stepped surface model of ZnO.

Supplementary Text

S-III. DSC and TG curves of AP with T-ZnO and R-ZnO

Pure AP and mixtures of AP with ZnO additives were characterized by TG-DSC using Diamond TG/DSC in N_2 atmosphere over the temperature range of 30-500°C with lids to investigate the catalytic activity of ZnO nanocrystals in the thermal decomposition of AP. A total sample mass of 3.0 mg was used for all runs. The weight ratio of ZnO additive to AP was 2:100 and the heating rate was 10 K/min. In addition, the activation energies of AP decomposition with ZnO additives were measured by varying the heating rates from 2 to 20 K/min. Figure S3 shows the DSC curves of AP with and without

involving the as-prepared ZnO nanocrystals. The decomposition of pure AP underwent a two-stage process. The first endothermic peak at 243°C was due to the crystal transformation of AP from orthorhombic to cubic phase, while the second exothermic peaks occurred at temperature of 300°C was attributed to the LTD of AP, and the third exothermic peaks occurred at temperature of 380°C was attributed to the HTD of AP. The thermal decomposition of pure AP, depending on the quality of crystals, granularity, and heating with or without lids, usually undergoes two or more steps.[12-14] For the present work, it is surprising that, when AP was mixed with the as-prepared ZnO nanocrystals, the decomposition peaks of HTD and LTD were almost overlapping as shown in Figure S3. In the case of the additives of T-ZnO, the sole decomposition process showed a peak temperature at 294°C, meaning that the HTD were reduced by 86°C. For R-ZnO as the additives, the HTD temperature was decreased to 296°C. From the integral area of the exothermic process, the decomposition heat of AP was determined. It showed a decomposition heat of 1065 $J \cdot g^{-1}$ with lids for pure AP. Strikingly, for the T-ZnO and R-ZnO as the additives, the decomposition heat of AP was increased to 1812 and 2160 $J \cdot g^{-1}$ with lids, respectively.

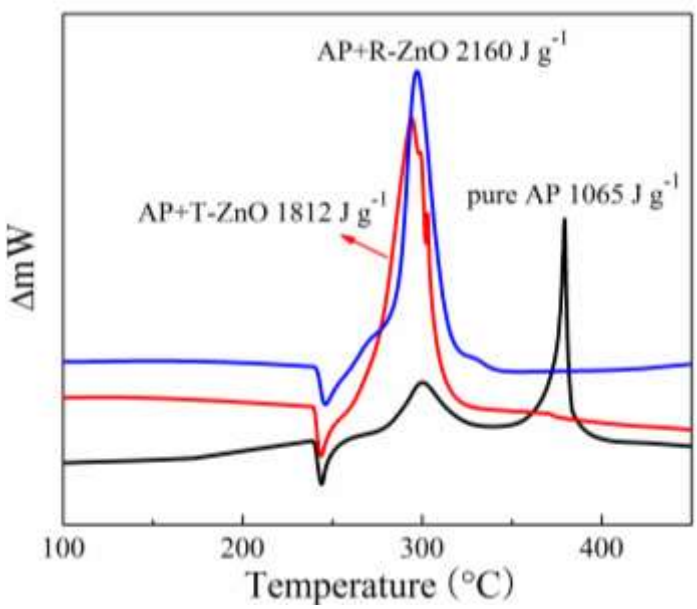

Figure S3. DSC curves of pure AP and mixture of AP with nano-ZnO measured using ceramic pans with lids at heating rate of 10 K min^{-1}

This journal is © The Royal Society of Chemistry 2013

The performance of nano-ZnO in the thermal decomposition of AP was investigated by TG measurements with a heating rate of 2-20 $K \cdot min^{-1}$. Two stages mass loss were observed for both pure AP and mixture of AP with nano-ZnO from room temperature to 500°C. From Figure S4, the first stage corresponding 30 percent weight loss was attributed to the partial decomposition of AP, and the second stage associated with 70 percent weight loss was caused by the complete decomposition of the intermediate to volatile products for pure AP. In the presence of nano-ZnO catalyst, in which affect mainly the initial period of reaction, the transformation degree during thermal decomposition of AP reaches above 70 percent, while non-catalyzed decomposition was usually limited by the level of 30 percent. Kinetic parameters for AP decomposition with ZnO additive was calculated from the exothermic peak temperature dependence as a function of heating rate. Figure S4 (a) and (b) show the TG curves of pure AP and mixture of AP with nano-ZnO at different heating rates in ceramic crucibles without lids, respectively. It can be seen from Figure S4 that the decomposition temperature was dependent on the heating rate.

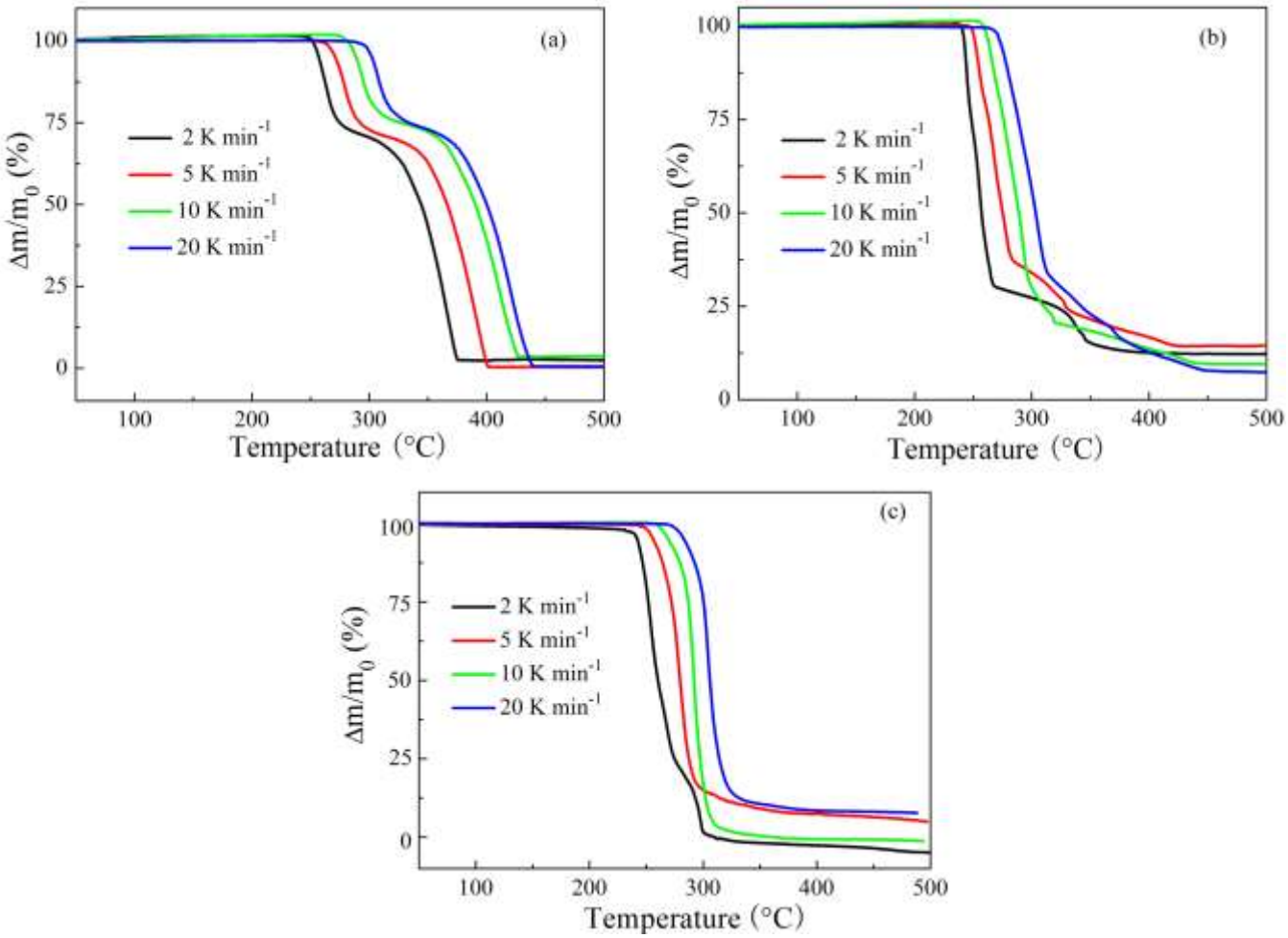

Figure S4. TG curves measured using ceramic pans without lids for pure AP (a), mixtures of AP with T-ZnO (b) and R-ZnO (c) that were conducted at different heating rates.

S-IV. PA adsorption and Dissociation on ideal $(10\bar{1}0)$ surface

For the relaxed ZnO $(10\bar{1}0)$ slab, oxygen atoms on the surface stick slightly out of plane. Three possible adsorption configurations were considered for $HClO_4$ adsorption, as shown in Figure S5(a). The adsorption energies for these three geometries are -0.20 eV, -0.09 eV and -0.18 eV respectively, which indicate the adsorption of AP on the ZnO $(10\bar{1}0)$ is relatively weak. The most stable ground state corresponds to a configuration where two oxygen atoms in the percolate making bonds with two Zn atoms on the surface.

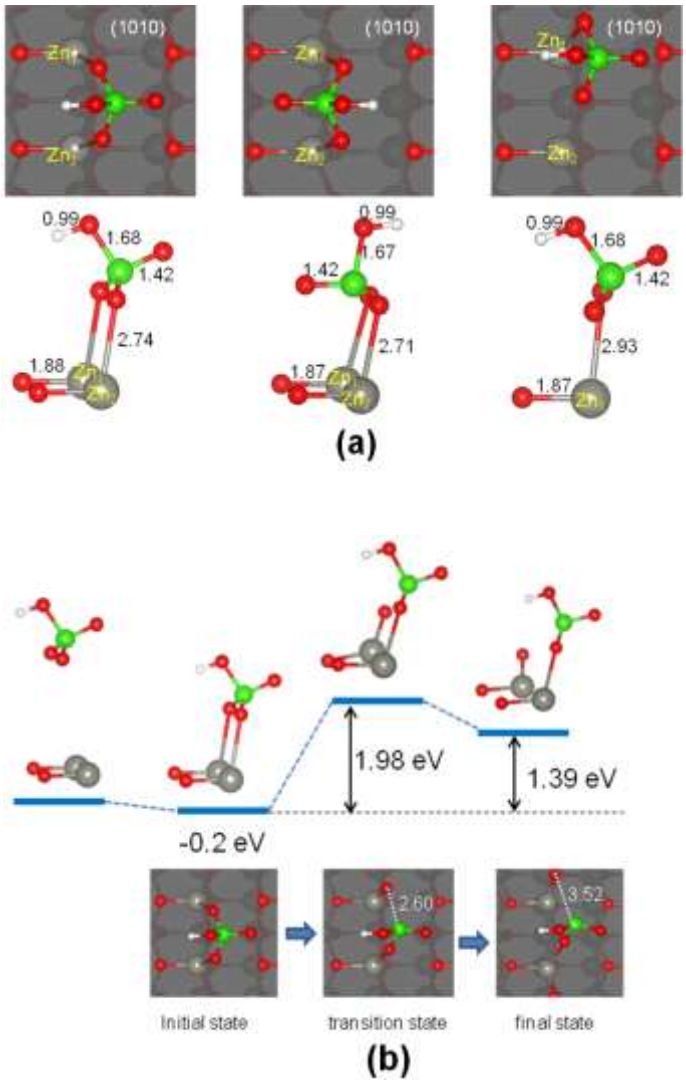

Figure S5. (a) and (b) indicates adsorption geometries and dissociation path of $HClO_4$ on Zn (1010) facets.

Figure S5(b) shows the MEP for such process starting from the most stable adsorption geometry. The transition state corresponds to a mid-point along the pathway where O-Cl bond is partially broken while the oxygen atom is migrating over the top site to the more stable two-fold coordinated bridge site. The activation barrier deduced from the energy difference between transition state and initial state is 1.98 eV, which is relatively high. This indicates that such decomposition process seems to be impractical on an ideal ZnO $(10\bar{1}0)$ surface.

Reference:

(1) B.L. Zhu, C.S. Xie, A.H. Wang, D.W. Zeng, W.L. Song, X.Z. Zhao. The gas-sensing properties of thick film based on tetrapod-shaped ZnO nanopowders. Materials Letters, 2005, 59, 1004–-1007.

(2) Bin Liu, Hua Chun Zeng. Hydrothermal Synthesis of ZnO Nanorods in the Diameter Regime of 50 nm. J. Am. Chem. Soc. 2003, 125, 4430-4431

(3) G. Kresse, J. Hafner. *Phys. Rev. B* **1993**, *47*, 558.

(4) G. Kresse, J. Hafner. *Phys. Rev. B* **1994**, *49*, 14251.

(5) G. Kresse, J. Hafner. *Comput. Mater. Sci.* **1996**, *6*, 15-50.

(6) G. Kresse, D. Joubert. *Phys. Rev. B* **1999**, *59*, 1758.

(7) J. P. Perdew, S. Burke, M. Ernzerhof. *Phys. Rev. Lett.* **1996**, *77*, 3865.

(8) G. Henkelman, H. Jónsson. *J. Chem. Phys.* **2000**, *113*, 9978.

(9) G. Henkelman, B. P. Uberuaga, H. Jónsson. *J. Chem. Phys.* **2000**, *113*, 9901.

(10) T. Akiyama, A. J. Freeman, K. Nakamura, T. Ito. *J. Phys.: Conf. Ser.* **2008**, *100*, 052056.

(11) J. H. Song, T. Akiyama, A. Freeman. J. *Phys. Rev. B* **2008**, *77*, 035332.

(12) T. G. Devi, M. P. Kannan, B. Hema. *Thermochim. Acta* **1996**, *285*, 269.

(13) S. Vyazovkin, C. A. Wight. *Chem. Mater.* **1999**, *11*, 3386.

(14) D. Majda, A. Korobov, U. Filek, B. Sulikowski, P. Midgley, D. Vowles, J. Klinowski. *Chem.* Phys. Lett. **2008**, 454, 233.